Evaluating Cardiac Strains from One and Two Short-Axis Slice Models Based on DENSE and Cine MRI

Augusto Delavald Marques[1 [0000−0002−3297−4761]], Mohammad Naqizadeh Jahromi[1 [0009−0008−7045−4848]], Luigi Wellner[1 [0009−0001−2116−4739]], Ariel J. Hannum[2−5 [0000−0003−0650−574X]], Zhan-Qiu Liu[2,3 [0000−0002−6873−9501]] Dazhong Wu[1 [0000−0002−0215−4906]], Daniel B. Ennis[2−5 [0000−0001−7435−1311]], and Luigi E. Perotti[1 [0000−0002−9010−2144]]

[1] Department of Mechanical and Aerospace Engineering, University of Central Florida, Orlando, FL, United States
Luigi.Perotti@ucf.edu
[2] Department of Radiology, Stanford University, Stanford, CA, United States
[3] Division of Radiology, Veterans Administration Health Care System, Palo Alto, CA, United States
[4] Cardiovascular Institute, Stanford University, Stanford, CA, United States
[5] Department of Bioengineering, Stanford University, Stanford, CA, United States

Abstract. Cardiac strains are important biomarkers of cardiac performance. Regional strain calculation from Cine MR images would facilitate their clinical adoption and obviate the need for acquiring specialized images. In this work we investigate three models to compute mid-ventricular cardiac strains. The first model is based on two short axis DENSE MRI slices, which provide voxelwise displacements, i.e., a complete description of the myocardial deformation. The second model is based on one DENSE slice, where we investigate the effect of reduced displacement information – but faster data acquisition – on the computed strains. The third model is based on one short-axis Cine slice, which is among the fastest and most common MRI data acquired in cardiac exams. To validate the three models and the underlying kinematic assumptions, we use a simple and previously developed computational cardiac phantom. Subsequently, we compare the proposed models using data from healthy volunteers (N=10), where we consider the results from the two-slice DENSE model as the most reliable since they are computed from the complete voxelwise displacement field. All models are evaluated using circumferential and longitudinal strains. Although all models agree well with the ground truth analytical solution when images are generated from the phantom, discrepancies emerge as the models are applied to real data: the one-slice DENSE model tends to significantly underestimate longitudinal strains while the one-slice Cine model overall underestimates epicardial circumferential strains. These differences are discussed in terms of the models' characteristics together with possible future improvements.

Keywords: Cardiac strains · Cardiac kinematics · DENSE MRI · Cine MRI · Kinematics models

1 Introduction

Cardiac strains are useful indicators of cardiac performance, with both regional and global strain metrics offering a measure of myocardial health. These measures can assist in distinguishing normokinetic, hypokinetic, dyskinetic, and hyperkinetic myocardium, which has utility in several cardiomyopathies. Despite their clinical usefulness, these measures are still not widely adopted. A primary challenge lies in the data availability for robustly and reliably computing strains. Different MR images have diverse image-contrast and types of information that can facilitate the building of patient-specific models. Displacement Encoding with Stimulated Echoes (DENSE) [13] MR images provide voxel-wise displacements throughout the cardiac cycle, but are less frequently acquired due to time and cost despite DENSE accuracy and precision. Conversely, Cine MR images are acquired for all cardiac MRI exams and are faster and simpler to acquire. Many methods have been proposed to use either Cine (e.g., [10,7]) or DENSE (e.g.,[13,3]) MRI data to compute cardiac strains. Several studies have also combined kinematics information from DENSE MRI with Cardiac Diffusion Tensor Imaging — a technique to measure cardiac microstructure information — to compute myofiber strains (e.g., [9,14]), a biomarker directly linked to cardiac contraction and relaxation.

While previous studies have made significant progress in automatically and efficiently computing cardiac strains, there is still the need to develop and evaluate methods that can leverage a reduced number of images and/or images routinely acquired in a clinical setting, e.g., short axis Cine MRI data. The goal of this study was to build and compare image-based models to compute mid-ventricular cardiac strains based on one or two slices of DENSE or Cine MRI data.

2 Method

We will focus on circumferential E_{cc} and longitudinal E_{ll} strains, as those strain components are computed more reliably. Three models will be constructed: 1) A model based on two DENSE short-axis slices; 2) A model based on one DENSE short-axis slice; and 3) A model based on one Cine MRI slice. The models are ordered from the more complete – but also the most complex in terms of image acquisition – to the one using the most commonly available and least amount of information (the one-slice Cine model). The proposed models are first tested using a computational cardiac phantom where ground truth information is known. Subsequent testing uses MRI data acquired in healthy volunteers. In the following, the models are described first, followed by a brief description of the computational phantom and acquired image dataset to validate and test the proposed strategies.

2.1 One and Two Slice Models

The DENSE two-slice model uses full displacement information to compute cardiac strains. In this case, radial basis functions (RBF) are employed to interpolate the voxelwise displacement data and compute a continuous displacement field $\mathbf{U}(\mathbf{X})$. The deformation gradient tensor can then be computed at any point in the myocardium as $\mathbf{F} = \nabla_{\mathbf{X}}\mathbf{U} + \mathbf{I}$. Finally, the Green-Lagrange strain tensor $\mathbf{E}$ is computed as $\mathbf{E} = \frac{1}{2}\left(\mathbf{F}^{\mathrm{T}}\mathbf{F} - \mathbf{I}\right)$ and projected along the circumferential ($\mathbf{c}$) and longitudinal ($\mathbf{l}$) directions to evaluate circumferential $\mathrm{E_{cc}}$ and longitudinal $\mathrm{E_{ll}}$ strains, respectively.

The second, one-slice model requires only a single DENSE short-axis slice and compensates for the missing displacement data (i.e., the displacement gradients in the longitudinal direction) by using a kinematic assumption. Using one-slice displacement data, it remains feasible to interpolate the displacements $\mathbf{U}(\mathbf{X})$ in the X and Y directions using RBF, and compute the components $F_{i,\alpha}$ of the deformation gradient tensor ($i = 1, 2, 3$ and $\alpha = 1, 2$). These components are sufficient to compute $\mathrm{E_{cc}}$, since the circumferential vector $\mathbf{c}$ lies in the XY (slice) plane. In order to compute $\mathrm{E_{ll}}$, since the components $F_{i,3}$ are not available, we assume that the myocardium is incompressible, a reasonable approximation given the myocardium low compressibility [12,16,6]. Based on this assumption, the myocardial volume V can be approximated as,

$$V = h_{\mathrm{ref}} A_{\mathrm{ref}} = h_{\mathrm{t}} A_{\mathrm{t}} \,, \tag{1}$$

where h and A are the slice height and the area in the reference configuration and at time t. A related approach based on preserving voxel volumes has been previously adopted in [8].

Using Eq. (1), $h_{\mathrm{t}}/h_{\mathrm{ref}} = A_{\mathrm{ref}}/A_{\mathrm{t}}$ and $\mathrm{E_{ll}}$ can be approximated as,

$$\mathrm{E_{ll}} = \frac{1}{2}\left[\left(\frac{A_{\mathrm{ref}}}{A_{\mathrm{t}}}\right)^2 - 1\right] . \tag{2}$$

Another possibility consists in computing $\mathrm{F_{33}}$ by imposing $\det(\mathbf{F}) = 1$ and assuming $F_{\alpha,3} = 0$ (neglecting the slice torsion) as done in [11]. However, the calculation of $\det(\mathbf{F})$ involves cubic terms and may be very sensitive to the noise in the data; therefore we do not use this approach in the current work.

The last model is based on one, short-axis, Cine slice. In this case, voxel-wise displacements are not available and cannot be interpolated using RBF. As in the one-slice DENSE model, Eqs. (1) and (2) are used to compute $\mathrm{E_{ll}}$ and a similar approach is adopted to estimate average (contour) $\mathrm{E_{cc}}$ values at epicardium and endocardium per timeframe, i.e.,

$$\mathrm{E_{cc}} = \frac{1}{2}\left[\left(\frac{p_{\mathrm{t}}}{p_{\mathrm{ref}}}\right)^2 - 1\right] , \tag{3}$$

where p_{ref} and p_{t} are the length of the endocardial or epicardial contour in the reference configuration and at time t, respectively.

2.2 Phantom Model

The mid-ventricular idealized phantom developed in [14] was used to test the proposed models. The phantom consists of an axial symmetric, time-resolved, cylindrical geometry with a parametrized deformation mapping $\boldsymbol{\varphi}$ in the radial, circumferential, and longitudinal directions. The phantom's endocardial and epicardial radii at the beginning of systole are set to 25mm and 35mm, and short axis slices were generated at $Z = 8$mm and $Z = 16$mm. In order to mimic the volunteers' imaging protocol, the phantom short-axis slices spatial resolution was set to $2.5 \times 2.5 \times 8\text{mm}^3$ and a simple four-point encoding [17] was simulated, instead of the balanced four-point encoding used in the original phantom [14]. The phantom provides ground truth analytical displacements and strain maps for all cardiac phases against which the different models were tested. For simulating Cine images, the voxels were ignored, and only the epicardial and endocardial contours were considered.

2.3 Imaging Data and Image Processing

The dataset included 2D balanced steady state free precession (bSSFP) Cine and DENSE images acquired in healthy volunteers (N=10 - 4 Male/ 6 Female 36.3 ± 12.4 years old: IRB approval; after consent – Stanford Administrative Panel on Human Subjects in Medical Research, Reference #FWA00000929 & #FWA00000934). Cardiac bSSFP Cine scans were ECG-gated and breath-held with the following parameters: resolution = $1.2\times1.2\times8\text{mm}^3$, temporal resolution = 30ms, flip angle = 10-30 degrees, bandwidth = 997Hz/Px, TE = 1.337ms, TR = 32ms, matrix = 256×216, acceleration = GRAPPA×3, number of reference lines = 45 integrated lines, FOV = 300×253. If necessary, phase oversampling was utilized to reduce aliasing artifacts. Breath-hold duration was between 12-20s. Cardiac DENSE scans were also ECG-gated and breath-held with the following parameters: resolution = $2.5\times2.5\times8\text{mm}^3$, temporal resolution = 15ms, flip angle = 15 degrees, xyz-displacement encoding with simple 4-point encoding strategy and 3-pts phase-cycling anti-echo suppression, displacement encoding frequency $k_e = 0.10$cycles/mm, through-plane dephasing frequency $k_d = 0.08$cycles/mm, TE = 1.26ms, TR = 15ms, matrix = 48×48, rFOV = 120×120. Breath-hold duration was between 12-20s.

A central frequency scout sequence was utilized at first to find the best central frequency that yielded minimal artifacts over the LV. Two subsequent midventricular slices were selected to construct the presented models.

The open-source DENSE-analysis processing software [13,4] was used to process the DENSE images and compute voxelwise displacements, which constitute the input for the one and two slice DENSE models described in Sec. 2.1. Cine images corresponding to the same mid-ventricular locations of the selected DENSE slices were automatically segmented using a machine-learning model [15].

3 Results and Discussion

We started by comparing E_{cc} and E_{ll} computed in the phantom model (ground truth) and using the generated DENSE and Cine images (Fig. 1) using the exact segmentation and voxel displacement information, i.e., excluding the effect of the processing due to the DENSE-analysis software and the machine learning segmentation of Cine images. In the DENSE-based models shown in Fig. 1, strains are computed at four equidistant transmural locations along lines separated by 10°. In the one-slice Cine model, strains are computed at 72 equidistant points distributed on the endocardium and epicardium contours (36 on each contour). In this case, the results obtained using the one and two-slice DENSE models agree well with the ground truth values of E_{cc} and E_{ll}. This shows that the simple RBF interpolation does not introduce significant error in the computed strains and that the approximation to compute E_{ll} is reasonable in simple case scenarios and when the segmentation is exact. Similar results are obtained using the model based on one Cine slice, where endocardial and epicardial E_{cc} and global E_{ll} agree well with the ground truth values. The median values computed at peak systole with the analytical phantom and the proposed models without the effect of the image processing pipelines are also included in Fig. 2.

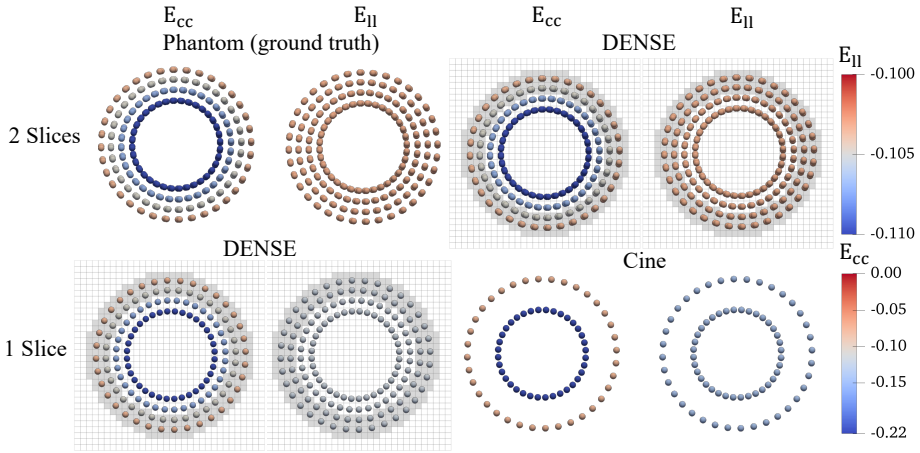

Fig. 1. Strain maps at peak systole in the analytical phantom (ground truth) and across the proposed models without including the effect of the image processing pipeline, i.e, based on exact image segmentation and displacement voxel values.

To study the effect of the image processing pipeline, i.e., the DENSE-analysis processing software, we generated images from the phantom with SNR values equal to 10, 20, and infinity. As before, the models were also solved using the exact image segmentation and voxel values for comparison (Phantom one and two slice DENSE models in Fig. 2). The computed E_{cc} and E_{ll} values

for all models agree well at peak systole, although there is a slight overestimation/underestimation (in magnitude) of epicardial/endocardial E_{cc} in both the two-slice and one-slice DENSE models. This bias in the computed E_{cc} may be due to the interpolation performed to extract displacement information from DENSE phase data during image processing. An overestimation (in magnitude) in E_{ll} is also observed in the one-slice DENSE and Cine models, which employed Eq. (2) and are based on manual segmentation. The larger (in magnitude) E_{ll} may be due, in part, to the fact that both methods based on one slice imaging data do not account for torsion during cardiac motion.

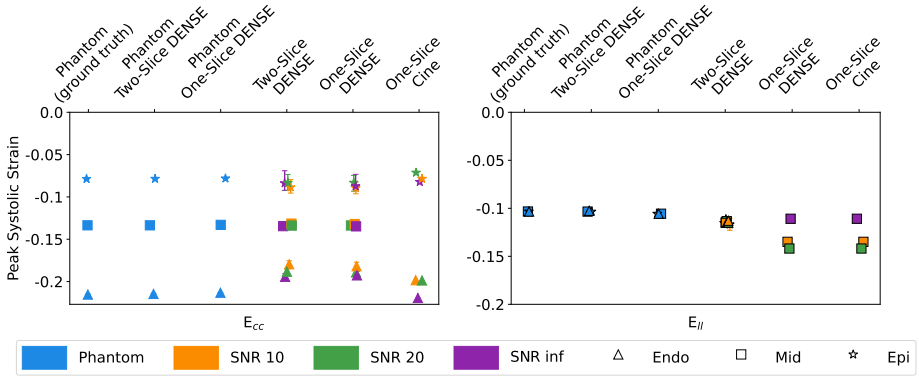

Fig. 2. Peak systolic strains across the proposed models without (phantom models) and with (models with SNR) the effect of the image processing pipeline. Values are reported with their respective IQR (when present). In this validation case, E_{ll} computed from both DENSE and Cine one-slice models is equal as it is computed from the same image segmentation obtained in the DENSE-analysis processing software (no machine learning model is adopted for segmenting the Cine image and the epicardial and endocardial contours from the DENSE image segmentation are directly used).

To test the proposed models with real data and throughout the cardiac cycle, we computed group-wide E_{cc} and E_{ll} values using imaging data from ten healthy volunteers (Fig. 3). For each volunteer dataset, we constructed one two-slice model and the corresponding two one-slice DENSE and Cine models when presenting the results. For both strain components, median and IQR (across all computed strain values) are reported in Fig. 3, together with epicardial and endocardial values for E_{cc}. Both one and two-slice DENSE models lead to a close group-wide median for E_{cc} at the epicardium while the one-slice Cine model underestimates E_{cc} at this location (Fig. 3, left). All models (two-slice DENSE and one-slice DENSE and Cine models) agree well in terms of median E_{cc} at the endocardium (Fig. 3, center). Regarding E_{ll}, the two-slice DENSE model and one-slice Cine model lead to similar values while the one-slice DENSE model tends to underestimate (in magnitude) this strain component. This is most likely due

to errors in the DENSE slice segmentation, which significantly affect the value of E_{ll} computed using Eq. (2). Although both one-slice DENSE and Cine models are affected by the segmentation process, Cine images offer higher resolution and are easier to segment effectively. Additionally, the one-slice Cine model utilizes machine learning for segmentation. These factors help reducing the variability in E_{ll} computed using the one-slice Cine model with respect to the one-slice DENSE model.

The results computed using the proposed models differ also for the presence of oscillations during the cardiac cycle, especially in E_{ll}. The increased variability in computed E_{ll} for the one-slice models arises from the sensitivity of Eq. (2) to segmentation, as it is challenging to obtain a smooth and consistent myocardial area change throughout the cardiac cycle. The E_{cc} computed using one-slice Cine data can also exhibit a significant variability, but Eq. (3) utilizes only the contour length, making it less sensitive than Eq. (2), which is based on myocardial area and therefore is affected by variations in both contour length and wall thickness. In general, the lower image quality at the end of the acquisition window may also contribute to the increased variability toward the end of the cardiac cycle.

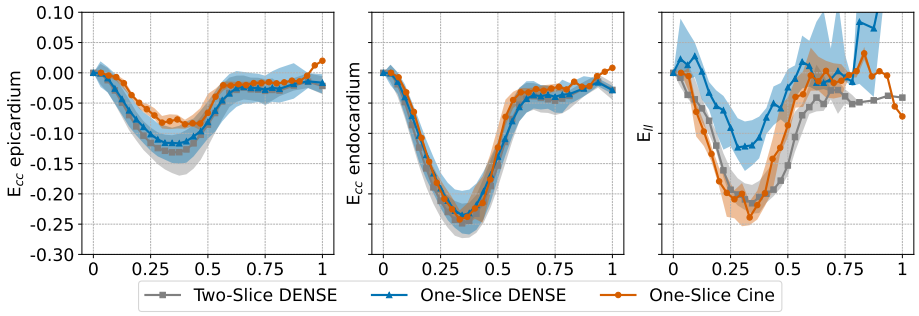

Fig. 3. Median strain values (continuous lines with markers) and their interquartile intervals (shaded regions) computed across all healthy volunteers (N=10) and using the proposed models. Strain values are reported with respect to normalized time: 0 corresponds to the beginning of systole and 1 to the end of the DENSE acquisition window (toward the end of the cardiac cycle).

To analyze the difference between the proposed models when individual volunteers are considered, we investigate peak systolic E_{cc} and E_{ll} strain values (Fig. 4). Among the models, the one-slice DENSE model showed more inter-subject variability for both E_{ll} and endocardial E_{cc}, while the two-slice DENSE model showed larger variability for epicardial E_{cc}. The mean of the absolute differences in E_{ll} between the two-slice DENSE and one-slice DENSE models at peak systole was equal to 10.3%, with a standard deviation of 4.3%. The mean of the absolute differences in E_{cc} between the two-slice DENSE and one-slice

DENSE models at peak systole was equal to 2.2%, with a standard deviation of 2.2% at epicardium, and 1.7% with a standard deviation of 1.8% at endocardium.

The mean of the absolute differences in E_{ll} between the two-slice DENSE and one-slice Cine models at peak systole was equal to 3.5%, with a standard deviation of 3.3%. The mean of the absolute differences in E_{cc} between the two-slice DENSE and one-slice Cine models at peak systole was equal to 5.5%, with a standard deviation of 2.9% at epicardium and 2.5% with a standard deviation of 1.3% at endocardium.

The one-slice DENSE and one-slice Cine models results shown in Fig. 4 were compared with the two-slice DENSE model for statistical significance. First, a Shapiro-Wilk test for normality was performed: if both datasets to be compared were normally distributed, then a paired samples t-test was conducted, otherwise, if at least one dataset was likely not normally distributed, the Wilcoxon signed-rank test was carried out. A significance level $\alpha = 0.05$ was selected in all tests. Regarding peak systolic endocardial E_{cc}, the Wilcoxon signed-rank test showed no significant differences between values computed with the one-slice DENSE model and the two-slice DENSE model (p=0.32) or between values computed with the one-slice Cine model and the two-slice DENSE model (p=0.37). Regarding peak systolic epicardial E_{cc}, no significant differences were detected by the paired samples t-test between values computed with the one-slice DENSE model and the two-slice DENSE model (p=0.10). However, a significant difference was detected by the paired samples t-test between values computed with the one-slice Cine model and the two-slice DENSE model (p=0.0003). Regarding peak systolic E_{ll}, no significant differences were detected by the Wilcoxon signed-rank test between values computed with the one-slice Cine model and the two-slice DENSE model (p=0.62). However, a significant difference was detected by the paired samples t-test between values computed with the one-slice DENSE model and the two-slice DENSE model (p=0.004).

A significant reason for the differences observed in E_{cc} and E_{ll} computed using the one-slice models may consist in the inaccurate segmentations of the Cine and especially DENSE short-axis slices. A possible next step to improve the consistency and quality of the DENSE short-axis segmentation is to adopt a machine learning framework for this task (e.g., the formulation previously proposed in [5]). Both Cine and DENSE one-slice model predictions can be improved by checking for inconsistencies across subsequent time-frames and correcting or filtering out incorrect segmentations (e.g., leading to large and unphysiological area differences between two subsequent time frames or significant short axis myocardial area decrease during contraction).

Additional extensions of the proposed comparisons and models include the calculation of radial strains and twist. Robustly computing radial strains from DENSE MRI remains challenging, and this hinders the comparison with values computed using the one-slice Cine model. Comparison analyses based on pseudo-images generated using a phantom with more complex geometry and motion can assist in developing and evaluating one- and two-slice models, including Cine only models. Developing more realistic – in terms of geometry and

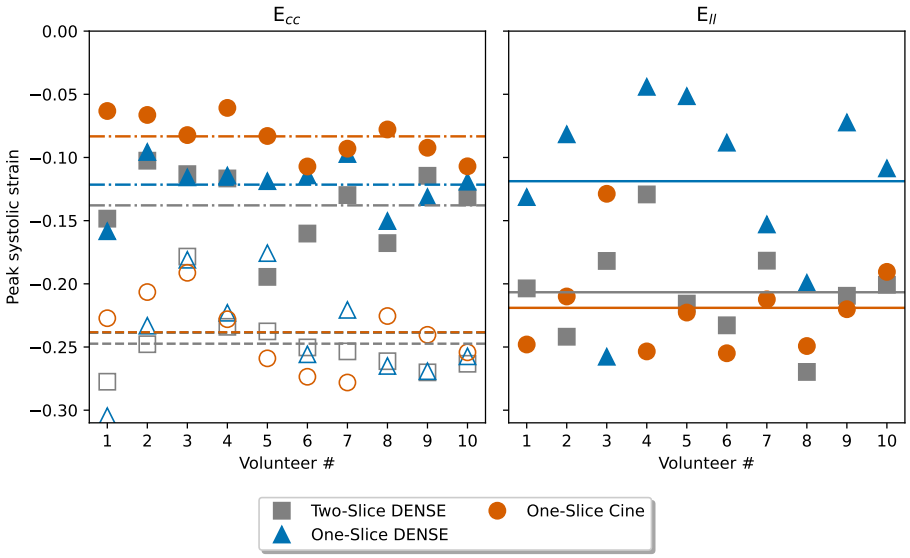

Fig. 4. Peak systolic median strains obtained using the proposed models per each volunteer. The lines represent the average of the median peak systolic strains across volunteers obtained with each model (dashed-dot lines refer to epicardial E_{cc}, dashed lines refer to endocardial E_{cc}, continuous lines refer to E_{ll}. For E_{cc}, filled markers refer to epicardial values, while empty markers refer to endocardial values).

motion – phantom models can also assist in evaluating twist calculations from the presented models. Finally, combining single slice image modalities (in our case DENSE and Cine MRI) and/or combining single slice images with computational models are other possibilities to improve the robustness of the computed strains and expand the type of kinematics measures (e.g., radial strain and twist) that can be computed [1,2].

4 Conclusions

In this work we have presented three different models to compute mid-ventricular cardiac strains from two and one short axis DENSE slices, and one short axis Cine slice. All models agree well with the ground truth data when synthetic images are generated from the computational phantom. However, differences arise in E_{cc} and E_{ll} computed from real data. E_{ll} computed using the one-slice DENSE model and both E_{cc} and E_{ll} computed using the one-slice Cine model depend directly on the accuracy of the image segmentation. Although significant differences still exist, especially in E_{ll} values, the proposed one-slice models contribute to the effort to compute cardiac strains when only reduced displacement information is available as, for example, it can be the case in a clinical setting. In general, the decision of the model to adopt depends on the available data and, if

the choice of the data to be acquired is available, on the tradeoff between strain accuracy, completeness (local strains versus only epicardial/endocardial contour strains), and acquisition time. Improving the machine learning pipelines adopted for short-axis slice segmentation and checking for consistency across subsequent time-frames are two possibilities to improve the presented one-slice models.

Acknowledgments. This material is based upon work supported by the National Science Foundation under Awards No. 2205043 to LEP and DW, and 2205103 to DBE.

Disclosure of Interests. The authors have no competing interests to declare that are relevant to the content of this article.

Accepted Version This version of the contribution has been accepted for publication, after peer review but is not the Version of Record and does not reflect post-acceptance improvements, or any corrections. The Version of Record is available online at: http://dx.doi.org/10.1007/978-3-031-94562-5_12. Use of this Accepted Version is subject to the publisher's Accepted Manuscript terms of use https://www.springernature.com/gp/open-research/policies/accepted-manuscript-terms.

References

1. Berberoğlu, E., Stoeck, C.T., Kozerke, S., Genet, M.: Quantification of left ventricular strain and torsion by joint analysis of 3D tagging and cine MR images. Medical Image Analysis **82**, 102598 (2022)
2. Castellanos, D.A., Škardová, K., Bhattaru, A., Berberoglu, E., Greil, G., Tandon, A., Dillenbeck, J., Burkhardt, B., Hussain, T., Genet, M., et al.: Left ventricular torsion obtained using equilibrated warping in patients with repaired tetralogy of Fallot. Pediatric cardiology **42**(6), 1275–1283 (2021)
3. Ghadimi, S., Abdi, M., Epstein, F.H.: Improved computation of Lagrangian tissue displacement and strain for cine DENSE MRI using a regularized spatiotemporal least squares method. Frontiers in Cardiovascular Medicine **10**, 1095159 (2023)
4. Gilliam, A.D., Suever, J.D., and contributors: DENSEanalysis (2021), https://github.com/denseanalysis/denseanalysis
5. Jahromi, M.N., Marques, A.D., Ahmed, M., Liu, Z.Q., Hannum, A.J., Ennis, D.B., Perotti, L.E., Wu, D.: An nnU-Net Model to Enhance Segmentation of Cardiac Cine DENSE-MRI Using Phase Information. In: 2024 IEEE 12th International Conference on Healthcare Informatics (ICHI). pp. 670–673. IEEE (2024)
6. Judd, R.M., Levy, B.I.: Effects of barium-induced cardiac contraction on large-and small-vessel intramyocardial blood volume. Circulation research **68**(1), 217–225 (1991)
7. López, P.A., Mella, H., Uribe, S., Hurtado, D.E., Costabal, F.S.: WarpPINN: Cine-MR image registration with physics-informed neural networks. Medical Image Analysis **89**, 102925 (2023)
8. Moghaddam, A.N., Saber, N.R., Wen, H., Finn, J.P., Ennis, D.B., Gharib, M.: Analytical method to measure three-dimensional strain patterns in the left ventricle from single slice displacement data. Journal of Cardiovascular Magnetic Resonance **12**(1), 33 (2010)

9. Moulin, K., Croisille, P., Viallon, M., Verzhbinsky, I.A., Perotti, L.E., Ennis, D.B.: Myofiber strain in healthy humans using DENSE and cDTI. Magnetic resonance in medicine **86**(1), 277–292 (2021)
10. Mukherjee, T., Keshavarzian, M., Fugate, E.M., Naeini, V., Darwish, A., Ohayon, J., Myers, K.J., Shah, D.J., Lindquist, D., Sadayappan, S., et al.: Complete spatiotemporal quantification of cardiac motion in mice through enhanced acquisition and super-resolution reconstruction. bioRxiv pp. 2024–05 (2024)
11. Perotti, L.E., Magrath, P., Verzhbinsky, I.A., Aliotta, E., Moulin, K., Ennis, D.B.: Microstructurally anchored cardiac kinematics by combining in vivo DENSE MRI and cDTI. In: Functional Imaging and Modelling of the Heart: 9th International Conference, FIMH 2017, Toronto, ON, Canada, June 11-13, 2017, Proceedings 9. pp. 381–391. Springer (2017)
12. Rodriguez, I., Ennis, D.B., Wen, H.: Noninvasive measurement of myocardial tissue volume change during systolic contraction and diastolic relaxation in the canine left ventricle. Magnetic Resonance in Medicine: An Official Journal of the International Society for Magnetic Resonance in Medicine **55**(3), 484–490 (2006)
13. Spottiswoode, B.S., Zhong, X., Hess, A.T., Kramer, C., Meintjes, E.M., Mayosi, B.M., Epstein, F.H.: Tracking myocardial motion from cine DENSE images using spatiotemporal phase unwrapping and temporal fitting. IEEE transactions on medical imaging **26**(1), 15–30 (2006)
14. Verzhbinsky, I.A., Perotti, L.E., Moulin, K., Cork, T.E., Loecher, M., Ennis, D.B.: Estimating aggregate cardiomyocyte strain using *In Vivo* diffusion and displacement encoded MRI. IEEE transactions on medical imaging **39**(3), 656–667 (2019)
15. Von Zuben, A., Perotti, L.E., Viana, F.A.: Anatomically-guided deep learning for left ventricle geometry generation with uncertainty quantification based on short-axis MR images. Engineering Applications of Artificial Intelligence **121**, 106012 (2023)
16. Yin, F., Chan, C., Judd, R.M.: Compressibility of perfused passive myocardium. American Journal of Physiology-Heart and Circulatory Physiology **271**(5), H1864–H1870 (1996)
17. Zhong, X., Helm, P.A., Epstein, F.H.: Balanced multipoint displacement encoding for DENSE MRI. Magnetic Resonance in Medicine: An Official Journal of the International Society for Magnetic Resonance in Medicine **61**(4), 981–988 (2009)